OXFORD UNIVERSITY PRESS | Human Molecular Genetics

Renal pathology in a mouse model of severe Spinal Muscular Atrophy is associated with downregulation of Glial Cell-Line Derived Neurotrophic Factor (GDNF)

Journal:	*Human Molecular Genetics*
Manuscript ID	HMG-2020-D-00286.R1
Manuscript Type:	2 General Article - UK Office
Date Submitted by the Author:	n/a

Complete List of Authors:	Allardyce, Hazel; University of Aberdeen College of Life Sciences and Medicine, Anatomy; University of Edinburgh, Euan MacDonald Centre for Motor Neurone Disease Research Kuhn, Daniela; Hannover Medical School, Institute of Neuroanatomy Hernandez-Gerez, Elena; University of Aberdeen College of Life Sciences and Medicine, Anatomy; University of Edinburgh Division of Medical and Radiological Sciences, Euan Macdonald Centre for Motor Neurone Disease Research Hensel, Niko; Hannover Medical School, Neuroanatomy, OE 4140; Hannover Medical School, Centre for Systems Neuroscience Huang, Yu-Ting; University of Edinburgh, Centre for Discovery Brain Sciences Faller, Kiterie; University of Edinburgh, Euan MacDonald Centre for Motor Neurone Disease Research Quondamatteo, Fabio; University of Glasgow, School of Life Sciences Gillingwater, Thomas; University of Edinburgh, Euan MacDonald Centre for Motor Neurone Disease Research Claus, Peter; Hannover Medical School, Institute of Neuroanatomy; Hannover Medical School, Centre for Systems Neuroscience Parson, Simon; University of Aberdeen College of Life Sciences and Medicine, Anatomy; University of Edinburgh Division of Medical and Radiological Sciences, Euan Macdonald Centre for Motor Neurone Disease Research
Key Words:	Non-neuronal, Kidney, Sclerosis, Nephrin, Collagen IV

Renal pathology in a mouse model of severe Spinal Muscular Atrophy is associated with downregulation of Glial Cell-Line Derived Neurotrophic Factor (GDNF)

Hazel Allardyce [1,2], Daniela Kuhn [3], Elena Hernandez-Gerez [1,2], Niko Hensel [3,4], Yu-Ting Huang [2,5], Kiterie Faller [2,5], Thomas H. Gillingwater [2,5], Fabio Quondamatteo [6], Peter Claus [3,4], Simon H. Parson [1,2] *

1, Institute of Medical Sciences, School of Medicine, Medical Sciences and Nutrition, University of Aberdeen, Foresterhill, Aberdeen, AB25 2ZD, Scotland, UK;
2, Euan Macdonald Centre for Motor Neurone Disease Research, University of Edinburgh, Chancellor's Building, Edinburgh, EH16 4SB, UK.
3, Hannover Medical School, Institute of Neuroanatomy and Cell Biology, OE 4140, Carl-Neuberg-Str. 1, 30625 Hannover, Germany.
4, Center for Systems Neuroscience (ZSN) Hannover, University of Veterinary Medicine, Hannover, Bünteweg 2, 30559 Hannover, Germany.
5, Edinburgh Medical School: Biomedical Sciences, College of Medicine & Veterinary Medicine, University of Edinburgh, George Square, Edinburgh, EH8 9AG, UK;
6, Anatomy Facility, School of Life Sciences, Thomson Building, University of Glasgow, University Avenue, Glasgow, G12 8QQ, UK.

*Corresponding Author:

Professor Simon H. Parson
Email: simon.parson@abdn.ac.uk
Telephone: +44 (0)1224 274328
Mail: Anatomy Rm 324 Suttie Centre, Foresterhill, University of Aberdeen, Aberdeen, AB24 3HF

Abstract

Spinal Muscular Atrophy (SMA) occurs as a result of cell-ubiquitous depletion of the essential SMN protein. Characteristic disease pathology is driven by a particular vulnerability of the ventral motor neurons of the spinal cord to decreased SMN. Perhaps not surprisingly, many other organ systems are also impacted by SMN depletion. The normal kidney expresses very high levels of SMN protein, equivalent to those found in the nervous system and liver, and levels are dramatically lowered by ~90-95% in mouse models of SMA. Taken together these data suggest that renal pathology may be present in SMA. We have addressed this using an established mouse model of severe SMA. Nephron number, as assessed by gold standard stereological techniques, was significantly reduced. In addition, morphological assessment showed decreased renal vasculature, particularly of the glomerular capillary knot, dysregulation of nephrin and collagen IV, and ultrastructural changes in the trilaminar filtration layers of the nephron. To explore the molecular drivers underpinning this process, we correlated these findings with quantitative PCR measurements and protein analyses of Glial Cell-Line Derived Neurotrophic Factor (GDNF), a crucial factor in ureteric bud branching and subsequent nephron development. GDNF levels were significantly reduced at early stages of disease in SMA mice. Collectively, these findings reveal significant renal pathology in a mouse model of severe SMA, further reinforcing the need to develop and administer systemic therapies for this neuromuscular disease.

Introduction

Spinal Muscular Atrophy (SMA), an autosomal recessive condition, is a leading global genetic cause of infant disability. As a consequence of mutation of the *Survival Motor Neuron 1* gene (*SMN1*), low cellular levels of the essential and cell-ubiquitously expressed survival motor neuron protein (SMN) are produced (1). In humans, this essential protein is expressed by two almost identical genes; telomeric *SMN1* and centromeric *SMN2*. While *SMN1* produces approximately 90% of functional, full length SMN protein, *SMN2*, which differs only marginally but results in alternative splicing of exon 7, produces only ~10% of full length SMN (2). In SMA, a deletion or loss-of-function mutation of the *SMN1* gene results in a significant loss of SMN. Low protein levels produced by *SMN2* ensure that the condition is not embryonically lethal, but rather gives rise to characteristic SMA pathology; degeneration of lower alpha motor neurons, leading to skeletal muscle denervation and atrophy (3).

Despite the selective vulnerability of motor neurons to low levels of SMN, the ubiquitous decrease in expression results in a systemic presentation. In addition to characteristic lower motor neuron death, non-neuromuscular pathologies have been described in both patients and animal models (4), including, but not limited to, defects in the cardiovascular system (5–9), lungs (10), liver (11–13), spleen (14,15), pancreas (16) and gastrointestinal system (17).

Expression of SMN in the adult human kidney is high, with similar levels to those found in the CNS and liver (18), both of which are significantly impacted in SMA. In mice, normal renal SMN expression is high in comparison with other peripheral organs, while severe SMA mouse models exhibit a dramatic 90-95% reduction of SMN protein in kidney, which further decreases as the disease progresses (19). Data from SMA patients revealed histopathological abnormalities including tubular injury and fibrosis, and abnormal serum profiles, suggesting impaired kidney function and renal tubular dysfunction (20). Moreover, clinical trials have highlighted cases of proteinuria in SMA patients prior to any drug treatment, indicating compromised renal function (21). However, these

studies shed little or no light on the cellular and/or molecular pathways involved. Importantly, the highly vascular kidneys develop almost completely prior to birth, and nephrogenesis cannot be re-initiated following its completion in the late embryonic/ early postnatal period (22,23).

Life changing treatments are now either available: antisense oligonucleotide Nusinersen (Spinraza, Biogen, Cambridge, MA); or are becoming available: gene therapy Onasemnogene abeparvovec Zolgensma (AveXis, Novartis, Chicago, IL) for affected patients, and deliver significant improvements in survival and quality of life (24). With the CNS as primary target, the ability of these therapies to address systemic pathologies (25,26), and particularly those which develop very early in life, remains largely unknown. By treatment of the neuronal pathology alone, it is likely that previously undiagnosed systemic defects may later arise in patients with extended survival. In particular, renal pathology, which may have been masked in early age, may surface due to cumulative renal stress as a result of increased blood volume and higher filtration needs in later life.

To characterise the cellular and molecular consequences of SMN deficiency on the renal system, we carried out a detailed morphological and molecular study of the kidney in the Taiwanese mouse model of severe SMA. We report significant structural and ultrastructural abnormalities, with a dramatic reduction in nephron number in the early postnatal kidney of SMA mice. These changes were associated with early onset pathology, namely glomerular sclerosis. In addition, vascular density was reduced and filtration layer markers collagen IV and nephrin (a marker of glomerular integrity) were dysregulated. Glial cell-line derived neurotrophic factor (GDNF), a known determinant of ureteric bud branching (27), was downregulated in early-symptomatic kidneys in this mouse model of severe SMA, and likely drives the dramatic decrease in nephron number described here. These data emphasise the need for early treatment of systemic defects, which will likely result in late morbidity if left unresolved.

Results

Postnatal development is defective in kidneys from a mouse model of severe SMA

No gross anatomical abnormalities in kidney were apparent at birth (P1: pre-symptomatic), but by P4 (early symptomatic) and P8 (late symptomatic) stages, there were notable variations in size and colour (Figure 1A). From P4 onwards, absolute kidney weight was significantly reduced in SMA mice compared with heterozygous control littermates (Het), **P <0.01 (Figure 1B). However, when kidney weight was expressed relative to body weight, there was a significant decrease in P4 SMA only (**P<0.01: Figure 1C), which is prior to the significant wasting and weight loss seen by P8. This is indicative of an intrinsic abnormality in kidney growth and development. Western blotting for SMN revealed a decrease of 68% (***P<0.001) in protein expression at early symptomatic P5, which further decreased to 82% (**P<0.01) of Het levels by late symptomatic P8 (Figure 1D and Supplementary Figure 1). Routine inspection of P8 H&E stained sections of kidney revealed no gross morphological abnormalities, however nephron density in SMA appeared to be low in comparison with Het kidney (Figure 1E-H). An increased renal capsular thickness in SMA mice was also noted, indicating fibrosis (Figure 2B and D). Further careful observation found accumulations of PAS-positive, hyaline casts in glomeruli of kidneys from the SMA mouse model, which were completely absent in Het kidneys (Figure 1I-L). These structures are consistent with glomerular sclerosis and frequently associated with hypoplastic nephropathology, and therefore warranted further study.

Nephron Number is Decreased in kidneys from the SMA mouse model

To properly assess nephron number, we turned to gold-standard, stereological methods. This systematic approach revealed a substantial and significant ~65% decrease in nephron number in kidneys from the SMA mouse model, compared with Het littermates (**P<0.01: Figure 2E). Specifically, kidneys from the SMA mouse model lacked nephrons in the most peripheral, cortical regions, where the youngest nephrons are found (Figure 2A-D), suggesting retarded nephrogenesis.

No nephrogenic debris, associated with nephron death and degeneration was present, suggesting a failure in nephron development.

These data suggest that low levels of SMN protein are associated with significantly decreased nephrogenesis in kidneys from the SMA mouse model. This is important, as such a decrease in nephron number cannot be compensated for postnatally.

Ultrastructural changes are present in kidneys from the SMA mouse model

With the decrease in nephron number and evidence of glomerular sclerosis described above, we next investigated the ultrastructure of the multipartite, glomerular filtration layer. We first assessed the tripartite lamina of the glomerular basement membrane, made up of the podocyte foot processes of the Bowman's capsule, collagen basement membrane and endothelial plasmalemma. We found increased evidence of localised areas of basal lamina lamellation in kidneys from the SMA mouse model at P5 (Fig 3A and C), however this was not significant in comparison with Het littermates, where some lamellation was also present. We next assessed podocytes and associated slit pores by quantifying the intersectional length between adjacent podocyte foot processes, and example images used for quantification are shown in Figure 3B and D. A small, but non-insignificant, decrease was apparent between mean slit length in Het and SMA groups, Figure 3E (ns, P>0.05). These observations may suggest early evidence of damage, associated with glomerular filtration defects, are present at the ultrastructural level at this early symptomatic stage.

Vascular Deficits are present in kidneys from the SMA mouse model

As vascular pathology is commonly described in a range of organs in both mouse models (5,28) and patients (29), we examined capillary beds in kidneys from the SMA mouse model.

PECAM-1 (platelet endothelial cell adhesion marker-1) immunofluorescence of endothelial cells indicated a gross reduction in capillary density, including decreased staining in the inner medulla and disorganised architecture in the cortical regions of P8 kidneys from the SMA mouse model (Figure 4A

and D). Closer inspection revealed a decreased microvascular density in the cortex (Figure 4B and E), with a significant reduction of ~40% in PECAM-1 staining density in kidneys from the SMA mouse model relative to Het tissue, (***P< 0.001: Figure 4G). Whole tissue western blotting confirmed a continual decrease in PECAM-1 in kidneys from the SMA mouse model, with expression at P5 decreased by 53.2% (*P<0.05) and further to 78.6% at P8 (***P<0.001), Figure 4H-I and Supplementary Figure 2. As PECAM-1 presents as 2 bands in all mice (Figure H and I), both bands were quantified to ensure the reliability of results.

Z-stacks of confocal images of nephrons, taken from similar areas to ensure they were at comparable stages of maturity, showed reduced glomerular capillary bed complexity in SMA nephrons. These had fewer capillary loops and were smaller in SMA model mice (Figure 4C and F). These observations suggest that the previously desribed pattern of reduced tissue vascularity and maturation is also a feature of kidney development, which likely further compromises renal function.

Slit diaphragm protein nephrin is dysregulated in kidneys from the SMA mouse model

Given the defects in the ultrastructure of the glomerular filtration membrane, we next investigated the molecular composition of this layer by staining for nephrin, a zipper-like protein that functions to maintain intersections between foot processes on the slit diaphragm (30). Nephrin expression is a biomarker for early podocyte injury, and loss has been shown to precede the development of glomerular lesions (31). Immunostaining revealed a dramatic reduction of almost 4-fold in expression of nephrin in individual mature glomeruli from kidneys from the SMA mouse model relative to Het (***P<0.001: Figure 5 A-C).

At a whole tissue level, western blotting revealed a ~30% decrease in nephrin expression at early-symptomatic P5, and a later increase of ~30% above levels of Het littermates at P8, Figure 5D-E and Supplementary Figure 3. Given the ongoing developmental changes in the kidney at this time, it is perhaps not surprising that these differences were not significant (ns, P>0.05). This dysregulation is likely associated with the changes in the ultrastructure of the slit diaphragm described above, as

changes in nephrin expression are characterised by narrowing of the slits on the diaphragm and related to disturbance of protein ratio of the ultrafiltration barrier (32,33).

Collagen IV is dysregulated in kidneys from the SMA mouse model

The basement membrane extracellular matrix protein collagen IV is dysregulated in many SMA tissues (5,14), and in the kidney functions as the second layer of filtration in the renal corpuscle. Immunofluorescence highlighted an altered distribution of collagen IV throughout kidneys from the SMA mouse model, with Het sections showing a regular and consistent expression in all basement membranes and a thin capsular layer surrounding the kidney. In contrast, kidneys from the SMA mouse model displayed a dramatic increase in the thickness of the collagen IV capsule, suggestive of fibrosis (Figure 6A and D). Conversely, intercellular, glomerular and tubular basement membranes displayed a decreased intensity of staining in SMA (Figure 6C-D and E-F). All photomicrographs were obtained using identical staining and image capture parameters to ensure consistency, and therefore variance in staining intensity is likely representative of changes in collagen IV expression.

Glial Cell-Line Derived Neurotrophic Factor (GDNF) expression is altered in early-symptomatic severe SMA model mice

To characterise molecular factors underlying the observed structural alterations and assess expression of genes relevant for kidney development, we performed a quantitative real-time PCR screening with pooled kidney samples from Het and SMA model mice, specifically at early symptomatic stage P4 (Figure 7A). Three targets showed up- or down-regulation, respectively: the POU transcription factor Brn1 (POU Class 3 Homeobox 3, POU3F3), the transcription factor Paired box 2 (Pax2) and Glial cell-line derived neurotrophic factor (GDNF). Targets were further analysed with cDNA samples from individual Het and SMA mice at P2 and P4 (Figure 7B). While Brn1 and Pax2 did not show altered regulation, GDNF transcripts were significantly down-regulated at P4, but not at P2. We additionally analysed protein levels of GDNF in SMA and heterozygous control samples

(Fig. 7C-D) by Western blotting. Secreted GDNF has a relative molecular weight of 15 kDa, whereas an unprocessed pro-form shows a molecular weight of about 70 kDa as a dimer. Post-translational processing of GDNF has been described including proteolytic cleavage and N-linked glycosylation (34). Multiple comparison tests revealed a significant difference of 15 kDa GDNF for the genotype as source of variation. Interestingly, the GDNF pro-form was upregulated in samples from SMA mice indicating an additional level of regulation. However, both GDNF transcript and protein levels show a decrease. GDNF is important for kidney development, since reciprocal signalling between GDNF and its receptor Ret is crucial for ureteric bud branching and therefore establishing accurate kidney morphology (35). Taken together these data suggest molecular, structural and functional defects likely to lead to changes in kidney filtration and the onset of kidney sclerosis in SMA.

Discussion

Spinal muscular atrophy (SMA) is a multisystem disease affecting most organs, which now includes the kidneys. Here, we report small kidneys, with a severely decreased nephron density and early signs of fibrosis and sclerosis, consistent with significant pathology in the renal system of severe SMA mice. Structural and ultrastructural defects were present, including reduced vascularity, dysregulation of key glomerular filtration barrier components nephrin and collagen IV, and evidence of basement membrane lamellation. Finally, we determined a decrease in expression of GDNF mRNA transcripts which may molecularly underpin the reduction in nephron density described.

The small size of kidneys from the SMA mouse model at early-symptomatic age is indicative of an intrinsic abnormality in early postnatal renal development. During the first two days of murine postnatal life, the rate of nephrogenesis is accelerated and a large number of new nephrons are produced, as the ureteric bud extends to the most peripheral layers of the developing kidney (23). This surge allows previously vacant areas to be occupied and establishes the final characteristic renal structure. Additionally between days P4-6, a further accelerated period of growth allows maturation of existing nephrons (36). Lack of normal growth observed in kidneys from the SMA mouse model may be the outcome of a failure or delay in the final surge of nephrogenesis and subsequent maturation. Delayed growth in SMA patients and mouse models has been demonstrated in the neuromuscular system (37) and the liver (11), therefore a delay in renal development is also likely.

Nephron number is prenatally determined in humans and in the early postnatal days in mice (22,23). Following termination of nephrogenesis, nephron number is at a maximum, and then gradually declines throughout life. We determined that SMA mice have a dramatic reduction in nephron density at P8, an age chosen to correlate with the formation of mature nephrogenic structures and therefore permitting accurate identification. Low nephron number in these mice is likely a consequence of genetic predisposition, as other factors associated with this pathology, including

intra-uterine growth restriction and low birth weight, are not characteristic of SMA (38–40). Microarray analysis of SMN patterning during renal development shows strong expression in the renal vesicle and weak expression in metanephric mesenchyme and S-shaped bodies (41), however its role in these stages of the developing nephron remains unknown. Kidneys from the SMA mouse model lacked nephrons in the most peripheral layers of the renal cortex, consistent with a delayed development hypothesis which may be explained by an inability of the ureteric bud to extend to the furthest cortical regions in the allocated timeframe. The decreased levels of GDNF mRNA and protein also reported may provide a causative link between SMN and low nephron density. Reciprocal signalling between GDNF (secreted by the metanephric blastema) and the Ret receptor (expressed in the ureteric bud) is crucial in the induction and continued branching of the ureteric bud, and is therefore a determinant of nephron density (27,35). GDNF loss or reduction is shown to cause formation of renal hypodysplasia (42), a phenotype reminiscent of the reduction in nephron density observed in these SMA model mice.

Investigation at the ultrastructural level uncovered evidence of localised areas of basal lamina lamination, more frequently observed in SMA mice. Lamellation is a common feature of Alport's disease caused by defects in particular collagen IV isoforms, specifically α3, α4 and α5 chains, and results in proteinuria and progressive loss of kidney function (43,44). Dysregulation of collagen IV is commonly reported in SMA (5,14). In the kidney, collagen IV is a vital extracellular matrix protein of the basement membranes, important in maintaining the structural framework and acting as the second layer of filtration in the glomerulus (45). Intercellular glomerular and tubular basement membranes displayed decreased expression, indicating a defective layer with increased likelihood of proteinuria due to an abnormal glomerular basement membrane. Due to the young age of the SMA mouse model, we were unable to measure proteinuria and determine compromised renal functioning because of inadequate urine volume, but this has recently been described in patients (21). Collagen IV also constitutes the renal capsule, which was substantially thicker in the kidneys

from the SMA mouse model, indicating a fibrotic structure surrounding the organ. Together these findings suggest a significantly altered ultrafiltration layer which correlate with reports of proteinuria in patients (21).

Nephrin is an important regulator of kidney development, mediating podocyte maturation and maintaining glomerular structure and integrity throughout life (46,47). This transmembrane protein is localised to the slit diaphragm layer and constitutes a porous scaffold, with nephrin strands spanning between adjacent podocyte foot processes (33,48,49). Consistent with a previous study (33), our measurements of podocyte slit length revealed foot processes in Het mice separated by a ~35-40nm wide slit. Although not significant, a slight decrease in slit length in kidneys from the SMA mouse model was apparent. Depletion of this anchoring protein commonly causes narrowing of the slits and is associated with proteinuria as a result of podocyte detachment (33,47). We report dysregulation of nephrin expression in kidneys from the SMA mouse model, with tissue analysis revealing an early-symptomatic decrease in expression, which later increased to above that of heterozygous littermate controls. At the glomerular level, a profound decrease in staining intensity of nephrin was noted at a late-symptomatic stage. From these data we suggest the interplay of two important factors; [1] downregulation followed by a later increase in expression may be due to the mouse model itself, as an increase in pro-inflammatory cytokines IL-1B and TNFα is known to cause the upregulation of nephrin expression (32,50). In this Taiwanese model of SMA, pro-inflammatory cytokines are markedly increased from early-symptomatic stages representing systemic inflammation in the animal (51). We suggest that systemic inflammation, especially at later stages of disease progression, may result in a secondary increase in nephrin expression from initially low to ultimately high levels as detected by tissue analysis; [2]) Varying results between single glomerular and whole tissue expression at late-symptomatic stage may be the result of protein translocation from membrane to cytoplasm, as described in other nephropathies (31,52,53). In diseased states, nephrin expression shifts from a consistent and linear pattern to a granular distribution, less clearly

localised to the glomerular basement membrane, which would cause a diminished fluorescent signal in comparison with normal nephrin localisation. As both nephrin loss and redistribution have been shown to precede the development of glomerular lesions (31), dysregulation may provide early evidence of glomerular injury in SMA mice.

Vascular deficits were evident in kidneys from the SMA mouse model, corresponding with previous findings of depleted capillary density in other tissues in mouse models and patients (5,8,28,54,55). As highly vascular organs the kidneys must maintain intricate vascular networks critical for proper functioning. Kidneys from the SMA mouse model displayed a significant decrease in microvascular density, with reduced glomerular capillary bed complexity. Renal vascularisation occurs synchronously with nephrogenesis (56), therefore a delay in nephrogenic development may cause a subsequent delay in the development of the renal vessels. Differing reports of vascular defects in SMA are thought to be the result of tissue specific downstream effects of SMN deficiency on the vasculature itself, and are commonly associated with tissue hypoxia (4). Chronic hypoxia in the kidneys is a progressive accelerator of chronic renal disease, with decreased renal oxygenation leading to matrix accumulation and inflammatory response, causing fibrosis and ultimately end-stage renal disease (57). The kidney, although well perfused, has poor oxygenation of the renal parenchyma due to its architecture and function (58). Further insult due to reduced capillary density in SMA may result in chronic hypoxia of the tissue, leading to initiation of a fibrotic cascade. The interplay of cardiac defects, low nephron number and decreased capillary density may cause a highly stressed renal environment, possibly culminating in hypertension and renal insufficiency in SMA.

Renal health and later prognosis are directly influenced by nephron number (59), and associations with blood pressure form the basis of understanding for hypertension and chronic kidney disease (60,61). Significant nephron deficits lead to a vicious cycle of further nephron loss through hypertrophy and hyperfiltration as remaining nephrons attempt to compensate, culminating in an

increasingly stressed renal environment (62). Consequences of a severe nephron deficit may not arise in young patients due to their small size and proportionally low blood volume, however with newly available therapies able to extend patient lifespan, renal pathology could manifest in later life. A deficit in nephron number, together with defects in the ultrafiltration layers indicate an organ with retarded development that will most likely result in functional deficits. Significantly, even with a systemic treatment administered as early as birth, no recovery of nephron density is possible due to the entirely embryonic timescale of nephrogenesis. This suggests that combinatorial, non SMN-related therapy may be required to combat kidney pathology.

Conclusion

Renal pathology is present in a severe mouse model of SMA from early postnatal life, likely consequential of aberrant kidney development. In correlation with a recent study that has described functional changes in SMA patient kidneys (20), our findings characterise preclinical morphological and molecular changes that may be responsible for later functional outcomes. Kidney pathology may have been masked previously due to early disease fatality, however with new therapeutic options that extend patient lifespan available, consequences could manifest. These data provide evidence of additional systemic organ pathology in SMA and emphasise the need for systemic and combinatorial therapies.

Materials and Methods

Taiwanese SMA Mouse Model and Tissue Processing

The Taiwanese mouse model of SMA represents a severe form of the disease (63,64). Taiwanese SMA mice were maintained as breeding pairs under standard scientific pathogen-free conditions in animal care facilities at the University of Edinburgh. All experimental protocols were approved by the University of Edinburgh research and ethics committee and carried out in accordance with a license from the United Kingdom Home Office under the Animals (Scientific Procedures) Act 1986. Offspring were homozygous for SMN Knockout, $SMN^{-/-}$; $SMN2^{tg/0}$, (SMA disease model) or heterozygous for SMN knockout, $SMN^{+/-}$; $SMN2^{tg/0}$ (control). Mice were retrospectively genotyped following standard PCR protocols. Day of birth was defined as postnatal day 1 (P1). Kidneys from experimental and control littermates were harvested at birth, P1/2; representing a pre-symptomatic stage, P4/5; early-symptomatic and P8; late-symptomatic, staged in terms of standard neuromuscular pathology. For histological analysis and immunofluorescence protocols, whole kidneys were dissected, fixed in 4% paraformaldehyde (PFA) for 4 hours and then stored in phosphate buffered saline (PBS). For western blotting, kidneys were submerged into dry ice immediately following dissection and stored at -80°C. Both groups were then transferred to the Institute of Medical Sciences, University of Aberdeen. Paraffin wax embedded kidneys were sectioned (8µm) and stained with a standard haematoxylin and eosin protocol for initial histological assessment.

For electron microscopy, kidneys were rapidly dissected to $1mm^3$ pieces in 4°C buffer (0.1M Na-cacodylate buffer supplemented with 2 mM $CaCl_2$, pH 7.4) and fragments were fixed in a solution of 2% glutaraldehyde + 4% PFA in 0.1Na-Cacodylate buffer supplemented with 2mM $CaCl_2$ for 24 hours. For expression analyses by qRT-PCR, kidneys were collected from P2 and P4 control and SMA mice at Hannover Medical School. All experimental protocols followed German animal welfare law and were approved by the Lower Saxony State Office for Consumer Protection and food Safety (LAVES, approval number 15/1774).

Stereology

Stereological fractionator/dissector combination methods were employed to ensure an accurate estimation of nephron number. A pilot study was conducted to determine both the total number of sections through a kidney and the mean maximal glomerular diameter, to allow an optimum section sampling fraction and dissector height to be chosen. Paraffin embedded kidneys, P8 (n=3), were exhaustively sectioned (5μm) in a coronal plane, with collection of every 12th ("reference" section) and 13th section ("look-up" section). Sections were stained with a modified Periodic Acid Schiff protocol (10 minutes periodic acid, 30 minutes Schiffs reagent, counterstained with haematoxylin (Sigma-Aldrich, 395B-1KT)), imaged on a Zeiss AxioScan Z1 slide scanner, and analysed using ImageJ software with a grid overlain. "Reference" and "look-up" sections of each pair were compared and only newly appearing glomeruli were counted. Using Cavalieri's principle, when multiplied by the inverse section sampling fraction provided an estimation of total glomerular number (65).

Immunofluorescence

Kidneys (P8) were cryopreserved in 30% sucrose solution with 0.1% sodium azide and embedded in a 1:1 solution of optimum cutting temperature compound (OCT) and 30% sucrose solution at -40°C. Coronal kidney sections (8μm) were air dried for 1 hour and underwent antigen retrieval by submersion in 10mM sodium citrate buffer at 90°C (20 minutes). Sections were incubated for 2 hours in blocking solution (0.4% bovine serum albumin (BSA), 1% Triton X-100 in 0.1M PBS) at 4°C and then overnight with primary antibody; polyclonal guinea-pig anti-nephrin (Acris BP5030, 1:50), polyclonal rabbit anti-collagen IV (Millipore AB756P, 1:100), polyclonal goat anti-PECAM-1 (R&D AF3628, 1:100) at 4°C. Slides were washed three times (2x 10 minutes in PBT (0.1M phosphate buffered saline (PBS) with 0.1% Tween-20), and once in 0.1M PBS). Sections were incubated with corresponding secondary antibodies; Alexa Fluor 594 goat anti-guinea pig IgG (H+L) (Invitrogen A11076, 1:250), Cy3 goat anti-rabbit IgG (H+L) (Invitrogen A10520, 1:250), Alexa Fluor 488 donkey anti-goat IgG (H+L) (Abcam ab150129, 1:250) for 2 hours at 4°C, with successive washes as before.

Sections were mounted using MOWIOL media (10% Mowiol (Sigma-Alrich, 81381), 20% glycerol, 50% 0.2M Tris buffer pH 8.5, 3% 1,4-diazobicyclooctance in distilled water) containing 4',6-diamidino-2-phenylindole (DAPI).

Immunofluorescent stained slides were imaged at various magnifications on an Upright Zeiss Imager M2 Fluorescent microscope (x4, x10 objectives) and Zeiss LSM710 inverted confocal microscope (x20, x40 and x63 objectives). All images were captured using Zeiss Zen Black software.

Quantification

Nephrin Density

Density of nephrin staining was conducted on x63 magnification confocal images of 18 single nephrons of each genotype, from SMA and HET kidneys (n=3). Images were edited on Zen software to the same parameters to decrease background staining. Images were converted into binary using ImageJ. Stained area was encircled by the oval selection tool to represent the glomerular area. Histograms provided a pixel count expressing black pixels in relation to white pixels. Total nephrin stained area (black pixels) was calculated relative to total glomerular area (black and white pixels).

PECAM-1 Density

PECAM-1 staining was similarly quantified using ImageJ on x20 confocal images. PECAM-1 positive cell area (black pixels) was expressed as a percentage of total field of view area on ImageJ.

Semi-quantitative Western Blotting

Kidneys, P5 and P8 (n=4), were extracted in RIPA buffer (Thermo Fisher, 89900) containing 2.5% Halt protease inhibitor cocktail (Sigma-Aldrich, P8340) on ice for 20 minutes, homogenised and then centrifuged at 14,000g for 30 minutes at 4°C. BCA assay was carried out to quantify protein concentration of each sample. Tissue lysates were diluted to 2.5µg/µl and added to a 1:4 dilution with SDS-PAGE Loading sample buffer 4x. Wells were loaded with 50µg of tissue lysate protein.

Proteins were separated by SDS-polyacrylamide gel electrophoresis on NuPage 4-12% BisTris Gels during 1 hour at 160V, then transferred to Immobilon-FL transfer membrane for 90 minutes at 30V. Reversible total protein stain was carried out using Li-COR Revert total protein stain and wash solution (Li-COR, 926-11011). Membrane was reverted using 0.1% sodium hydroxide in 30% methanol. Membranes were submerged in blocking solution (1:1 Thermo Scientific Sea Block Buffer and PBST) at room temperature for 1 hour, then incubated overnight at 4°C with primary antibody; monoclonal mouse anti-SMN (BD, 610646, 1:1600), monoclonal rabbit anti-nephrin (Abcam ab216341, 1:5000), polyclonal rabbit anti-CD31(Abcam ab28364, 1:500). Membranes were washed (4x 5 minutes) in PBS, then incubated for 1 hour at room temperature with corresponding secondary antibody; IRDye® 800CW Goat anti-mouse (Li-COR 925-32210, 1:10,000) or IRDye® 680RD Goat anti-rabbit (Li-COR 925-68071, 1:10,000). Membranes were washed as before and imaged using Li-COR Odyssey imaging system. Western blotting analysis was performed with Image Studio Lite Version 5.2.

For analyses of GDNF expression levels, kidneys of SMA and heterozygous control animals were collected at postnatal days P2 and P4 and homogenized for 5 min with a TissueLyser II (Qiagen) using tungsten carbide beads (Qiagen) lysed in RIPA buffer [137 mM NaCl, 20 mM Tris-HCl pH 7, 525 mM β-glycerophosphate, 2 mM EDTA, 1 mM sodium-orthovanadate, 1% (w/v) sodium-desoxycholate, 1% (v/v) Triton-X-100, with phosphatase (1:20) and protease inhibitor (1:50) cocktails (Roche)]. Samples were then centrifuged at 4°C (22,000 rcf) for 15 min. Concentration of proteins was determined by Pierce™ bicinchonic acid (BCA) Protein Assay kit. Same amounts of the samples were analysed on Western blots after SDS-PAGE. The following antibodies were used: Primary antibodies, monoclonal mouse anti-SMN (BD, 610646, 1:4,000) and monoclonal mouse anti-GDNF (Santa Cruz, B-8, sc-13147,1:500). Secondary antibody, HRP-linked anti-mouse IgG (GE Healthcare, 1:5,000). After western blotting, membranes were stained and imaged for subsequent densitometry and normalization. Before incubation with antibodies, blots were blocked with 5% (w/v) bovine serum albumin (BSA) in TBS-T. Detection of chemiluminescence was performed with Immobilon™ Western

HRP Substrate (Millipore). Densitometry of staining and chemiluminescent signal was carried out with LabImage 1 D (Intas).

Transmission Electron Microscopy

Two randomly selected kidney fragments of each sample, P5 (n=4), were washed in 0.1M sodium cacodylate (pH7.4) (3x 5minutes), transferred into 1:1 solution of 2% osmium tetraoxide and 0.2M sodium cacodylate on ice for 2 hours and washed in distilled water (3x 10 minutes). Specimens were dehydrated through a series of alcohols and changes of propylene oxide (3x 5 minutes), then incubated overnight in 1:1 propylene oxide and Epon solution. Samples were submerged in 100% Epon resin for 24 hours, 100% Epon resin with accelerator for 24 hours and then embedded in Epon resin. To ensure correct region was identifiable in sample, semithin sections (1μm) were cut, stained with toluidine blue and examined under a light microscope. Only blocks with at least 3 mature and centrally located glomeruli were selected. Ultrathin sections (~90nm) were cut, collected on grids, stained with methanolic uranyl acetate (3 minutes) and lead citrate (3 minutes) and examined using a JEOL 1200 EX running at 80kV. Images were captured on a Cantega 2Kx2K camera using Olympus ITEM software. To select representative glomeruli, viewing of the section always began at the left side of the section and moved to the right. The entire grid was reviewed to identify medullary tissue. The first 3 glomeruli located in closest proximity to the medullary tissue represented the most mature and were used in analysis. If no medullary tissue was present, glomeruli were selected from the central region of the section. All peripheral glomeruli were discounted due to their immature stage. Analysis of podocyte coverage of the basement membrane was conducted on x5000 magnification photomicrographs using ImageJ. Three regions of the podocyte layer adjacent to the Bowman's basal lamina of each glomerulus was assessed (3 glomeruli per kidney), with 5 consecutive images taken at each region. Regions imaged were equally distributed in the glomerulus. Using the freehand line tool, the total length of basement membrane visible and the

length of each podocyte was measured. Mean intersectional space between podocytes was calculated.

Quantitative real time PCR (qRT-PCR)

Total mRNA from kidneys, P2 and P4 (n≥3), was isolated using Qiagen RNeasy Plus Kit according to manufacturer´s instructions. cDNA synthesis and PCR was performed as previously described on StepOnePlus thermocycler (Applied Biosystems) (66). For normalisation, expression of the housekeeping gene peptidyl-prolyl cis-trans isomerase (Ppia) was used. The following primers were used (5´>3´): Pax2 (NM_011037.4) FWD GAAGCTACCCTACCTCCAC and REV GCACTATAATAATAAGGGGAACT, GDNF (NM_010275.2) FWD TGACCAGTGACTCCAATATGCC and REV CCGCTTGTTTATCTGGTGACCT, Brn1 (NM_008900.2) FWD AATGAAATGAAAATATGGACAG and REV CAAATTTATTTTCTCAATCAGC.

Statistical Analysis

Statistical analysis was carried out on GraphPad PRISM software (GraphPad Software Inc.). All data is presented as mean ± SEM. Statistical testing utilised unpaired, two-tailed *t*-tests, where * <P0.05, ** <P0.01 and *** P<0.001. For analyses of qRT-PCRs, 2-way ANOVA with Holm-Sidak´s multiple comparisons test was used.

Funding

This work was supported by grants from SMA Europe and an Anatomical Society PhD Studentship to S.H.P and H.A.; and the Deutsche Muskelstiftung [grant number E-2019-01] to P.C.

Acknowledgements

We would like to acknowledge the Microscopy and Histology Core Facility members; Kevin Mackenzie, Debbie Wilkinson, Gillian Milne and Lucy Wight at the University of Aberdeen, and Margaret Mullin at the Glasgow Imaging Facility, University of Glasgow, for their support, assistance and use of the facilities.

Author Contributions

H.A., S.H.P. and F.Q. designed the study.

Y-T.H. and K.F. maintained mouse colonies, dissected tissues and genotyped animals at University of Edinburgh, D.K. and N.H at the University of Hannover.

H.A., E.H.G., D.K., N.H performed experiments and analysed data.

H.A., S.H.P., D.K., P.C. and T.H.G. prepared the manuscript.

Conflicts of Interest

The authors have no conflicts of interest.

Abbreviations

SMA Spinal Muscular Atrophy

SMN Survival Motor Neuron protein

GDNF Glial cell-line derived neurotrophic factor

SMN1 Survival Motor Neuron gene 1

SMN2 Survival Motor Neuron gene 2

Het Heterozygous control littermates

PECAM-1 Platelet endothelial cell adhesion molecule 1

Brn1 POU Class 3 Homeobox 3

Pax2 Paired Box 2

IL1β Interleukin 1 Beta

TNFα Tumour necrosis factor alpha

Figure Legends

Figure 1: Postnatal kidney development is defective in severe SMA mice.

(A) Gross anatomy of kidneys, harvested from HET (left) and SMA (right) mice at pre-symptomatic (P1), early-symptomatic (P4) and late-symptomatic (P8) stages, respectively. Scale bar, 5mm. (B) Quantification of kidney weight from P1, P4 and P8 mice. (C) Quantification of kidney weight, relative to body weight from P1, P4 and P8 mice. P values were calculated using a two-tailed Student's t-test. Error bars, mean ± S.E.M. (n ≥ 5 mice per group). (D) Relative SMN levels from quantified western blots at P5, ***P, and P8, **P. Error bars, mean ± S.E.M. (n ≥ 4 mice per group). (E-H) Representative light microscopy images of entire kidney sections stained with H&E from HET (E) and SMA (G) mice at P8, scale 200µm. Higher magnification images of kidney sections from HET (F) and SMA (H) P8 mice that show no gross morphological abnormalities, scale 100µm. (I-L) Representative photomicrographs of PAS-stained glomeruli from P8 mouse kidneys. (I) Typical healthy glomerulus in P8 HET kidney, (J-L) Glomeruli from kidneys of the SMA mouse model depicting varying degrees of glomerulosclerosis. Increasing accumulation of amorphous, pink, hyaline material shown from minor (J) to major (L), highlighted by asterisk (*). Scale 50µm.

Figure 2: Nephron number is decreased in kidneys from SMA mice

Representative micrographs of PAS stained, coronally sectioned kidneys from HET (A) and SMA (C) P8 mice, scale 0.5mm. Higher magnification images of cortical regions in HET (B) and SMA (D), scale 300µm. Insert depicts lack of nephrons in the peripheral cortex of kidneys from SMA mice and arrow points to thickened renal capsule, scale 150µm. (E) Quantification of nephron number in kidneys of P8 HET and SMA mice, **P. P values were calculated using a two-tailed Student's t-test. Error bars, mean ± S.E.M. (n =3 mice per group).

Figure 3: Ultrastructural changes are present in kidneys from SMA mice

Electron micrographs of the basement membrane and podocyte foot processes from P5 kidneys from HET (A) and SMA (C) mice. In (A), black arrows show adjacent foot processes from a single podocyte. The basal lamina is highlighted by an asterisk (*). The white arrow in (C) points to a representative region of glomerular basement lamellation in kidneys from the SMA group. Representative images of P5 kidneys from HET (B) and SMA (D) mice, of podocyte foot processes and underlying basal lamina from which measurements of slit pore length were conducted. Scale 500nm. (E) Quantification of slit membrane length in HET and SMA animals, P=ns. P values were calculated using a two-tailed Student's t-test. Error bars, mean ± S.E.M. (n=4 mice per group).

Figure 4: Vascular deficits are evident in kidneys from SMA mice

Representative immunohistochemistry of kidneys from P8 mice, HET (A-C) and SMA (D-F), stained with platelet endothelial cell adhesion marker-1 (PECAM-1). Overview of renal microvasculature in kidneys from HET (A) and SMA (D) P8 mice, highlighting reduction in capillary density and disorganised architecture of vessels, scale 200µm. Higher magnification depicts decreased staining density of renal cortex in SMA (E) compared with HET (B), scale 50µm. Representative z-stack micrographs of glomerular capillary structure in kidneys from HET (C) and SMA (F) animals, depicting less structurally complex capillary loops in SMA mice, scale 10µm. (G) Quantification of staining intensity of PECAM-1. (H-I) Total PECAM-1 protein levels analysed by western blot and normalised to total protein at ages P5 (H), *P, and P8 (I), ***P. P values were calculated using a two-tailed Student's t-test. Error bars, mean ± S.E.M. (n ≥3 mice per group).

Figure 5: Slit diaphragm protein Nephrin is abnormal in kidneys from SMA mice

Representative immunohistochemistry of kidneys from P8 mice, HET (A) and SMA (B), mature glomeruli are labelled with Nephrin, scale 10µm. (A1-B1) Pixels reversed to show stained (black) area of the glomerulus, encircled to represent glomerular area compared to unstained (white) background from kidneys of P8 HET (A1) and SMA (B1) mice. (C) Quantification of Nephrin stained

area. (D-E) Total Nephrin protein levels analysed by western blot and normalised to total protein, at ages P5 (D) and P8 (E), P=ns. P values were calculated using a two-tailed Student's t-test. Error bars, mean ± S.E.M. (n ≥3 mice per group).

Figure 6: Collagen IV is dysregulated in kidneys from SMA mice

Representative immunohistochemistry of kidneys from P8 mice, HET (A-C) and SMA (D-F), stained with collagen IV. (A and D) Overview of renal cortex and renal capsule. (D) Increased staining density of the renal capsule in kidneys from SMA mice compared to HET (A), scale 100µm. (B and E) Internal glomerular and tubular basement membrane staining density is decreased in kidneys from SMA mice (E), compared to HET (B), scale 50µm. (C and F) Photomicrographs of single glomeruli also further highlight loss of collagen IV expression in glomerular basement membrane in kidneys from SMA mice (F), compared to Het littermates (C), scale 10µm.

Figure 7: Pre-symptomatic expression of genes and proteins relevant for kidney development

(A) Expression of targets for developmentally-relevant factors were pre-selected by a screening in heterozygous control (HET) and SMA mouse kidneys at P4 by quantitative real time PCR (qRT-PCR). For the screening, pooled samples (for number of samples in the pool, see n-values below) from several mice and litters were used in order to reveal targets with fold changes > 1.5 or < 0.6. Since we applied a screening approach in pooled samples first, no standard deviations were calculated. (B) Three factors found to be regulated in the screening were further analysed by qRT-PCR in individual tissue samples at P2 and P4. Glial cell-line derived growth factor (GDNF) was significantly down-regulated in SMA mice at P4. *P; 2-way ANOVA; Holm-Sidak´s multiple comparisons test; P2 control n=5, P2 SMA n=3, P4 control n=5, P4 SMA n=6. (C) GDNF and SMN protein expression was analysed by Western blotting in HET and SMA kidney samples. Processed GDNF with a relative molecular weight (M) of 15 kDa and an unprocessed pro-form of GDNF (70 kDa) were both detected.

(D) For normalization, membranes were stained with Ponceau S. (D) Densitometic analyses of signals revealed down-regulation of 15 kDa GDNF in SMA samples compared to HER (2way ANOVA with Sidak´s multiple comparisons; significant for genotype as source of variation, *P, n=6 for each HET and SMA). Moreover, the GDNF pro-form showed an significant upregulation (2way ANOVA with Sidak´s multiple comparisons; significant for genotype as source of variation, **P, n=6 for each HET and SMA; also significant for P4 as time point with *P) indicating an additonal level of regulation by differential proteolytic processing.

Supplementary Figure 1: SMN Semi-Quantitative Western Blot

Uncropped blots for detection of SMN expression in Het controls and kidneys from SMA mouse model in P5 (A) and P8 (B) animals. Molecular weight of SMN is labelled as 40kDa. Total protein stain was used for normalisation of protein levels and is shown for kidneys from Het controls and SMA mouse model at P5 (C) and P8 (D). n=4 mice per group.

Supplementary Figure 2: PECAM-1 Semi-Quantitative Western Blot

Uncropped blots for detection of PECAM-1 expression in Het controls and kidneys from SMA mouse model in P5 (A) and P8 (B) animals. Molecular weight of SMN is labelled as 130kDa. Boxes highlight area of band quantified in HET 1 and SMA 1 lanes. Both the dominant band and the minor band below was quantified for all lanes. Total protein stain was used for normalisation of protein levels and is shown for kidneys from Het controls and SMA mouse model at P5 (C) and P8 (D). n=4 mice per group.

Supplementary Figure 3: Nephrin Semi-Quantitative Western Blot

Uncropped blots for detection of Nephrin expression in Het controls and kidneys from SMA mouse model in P5 (A) and P8 (B) animals. Molecular weight of SMN is labelled as 37kDa. Total protein stain

was used for normalisation of protein levels and is shown for kidneys from Het controls and SMA mouse model at P5 (C) and P8 (D). n=4 mice per group.

References

1. Lefebvre, S., Bürglen, L., Reboullet, S., et al. (1995) Identification and characterization of a spinal muscular atrophy-determining gene. *Cell*, **80**, 155–165.
2. Lorson, C. L., Hahnen, E., Androphy, E. J., et al. (1999) A single nucleotide in the SMN gene regulates splicing and is responsible for spinal muscular atrophy. *Proc. Natl. Acad. Sci. U. S. A.*, **96**, 6307–6311.
3. Monani, U. R., Sendtner, M., Coovert, D., et al. (2000) The human centromeric survival motor neuron gene (SMN2) rescues embryonic lethality in Smn-/- mice and results in a mouse with spinal muscular atrophy. *Hum. Mol. Genet.*, **9**, 333–339.
4. Hamilton, G. and Gillingwater, T. H. (2013) Spinal muscular atrophy: going beyond the motor neuron. *Trends Mol. Med.*, **19**, 40–50.
5. Maxwell, G. K., Szunyogova, E., Shorrock, H. K., et al. (2018) Developmental and degenerative cardiac defects in the Taiwanese mouse model of severe spinal muscular atrophy. *J. Anat.*, **232**, 965–978.
6. Araujo, A. prufer de Q. C., Araujo, M. and Swoboda, K. J. (2009) Vascular Perfusion Abnormalities in Infants with Spinal Muscular Atrophy. *J. Pediatr.*, **155**, 292–294.
7. Møller, P., Moe, N., Saugstad, O. D., et al. (1990) Spinal muscular atrophy type I combined with atrial septal defect in three sibs. *Clin. Genet.*, **38**, 81–83.
8. Rudnik-Schöneborn, S., Vogelgesang, S., Armbrust, S., et al. (2010) Digital necroses and vascular thrombosis in severe spinal muscular atrophy. *Muscle and Nerve*, **42**, 144–147.
9. Shababi, M., Habibi, J., Yang, H. T., et al. (2010) Cardiac defects contribute to the pathology of spinal muscular atrophy models. *Hum. Mol. Genet.*, **19**, 4059–4071.
10. Schreml, J., Riessland, M., Paterno, M., et al. (2013) Severe SMA mice show organ impairment that cannot be rescued by therapy with the HDACi JNJ-26481585. *Eur. J. Hum. Genet.*, **21**, 643–652.
11. Szunyogova, E., Zhou, H., Maxwell, G. K., et al. (2016) Survival Motor Neuron (SMN) protein is required for normal mouse liver development. *Sci. Rep.*, **6**, 1–14.
12. Vitte, J. M., Davoult, B., Roblot, N., et al. (2004) Deletion of Murine Smn Exon 7 Directed to Liver Leads to Severe Defect of Liver Development Associated with Iron Overload. *Am. J. Pathol.*, **165**, 1731–1741.
13. Deguise, M. O., Baranello, G., Mastella, C., et al. (2019) Abnormal fatty acid metabolism is a core component of spinal muscular atrophy. *Ann. Clin. Transl. Neurol.*, **6**, 1519–1532.
14. Thomson, A. K., Somers, E., Powis, R. A., et al. (2017) Survival of motor neurone protein is required for normal postnatal development of the spleen. *J. Anat.*, **230**, 337–346.
15. Deguise, M. O., De Repentigny, Y., McFall, E., et al. (2017) Immune dysregulation may contribute to disease pathogenesis in spinal muscular atrophy mice. *Hum. Mol. Genet.*, **26**, 801–819.
16. Bowerman, M., Swoboda, K. J., Michalski, J. P., et al. (2012) Glucose metabolism and pancreatic defects in spinal muscular atrophy. *Ann. Neurol.*, **72**, 256–268.
17. Sintusek, P., Catapano, F., Angkathunkayul, N., et al. (2016) Histopathological Defects in Intestine in Severe Spinal Muscular Atrophy Mice Are Improved by Systemic Antisense Oligonucleotide Treatment. *PLoS One*, **11**, e0155032.
18. Coovert, D. D., Le, T. T., McAndrew, P. E., et al. (1997) The survival motor neuron protein in spinal muscular atrophy. *Hum. Mol. Genet.*, **6**, 1205–1214.
19. Groen, E. J. N., Perenthaler, E., Courtney, N. L., et al. (2018) Temporal and tissue-specific variability of SMN protein levels in mouse models of spinal muscular atrophy. *Hum. Mol. Genet.*, **27**, 2851–2862.
20. Nery, F. C., Siranosian, J. J., Rosales, I., et al. (2019) Impaired kidney structure and function in spinal muscular atrophy. *Neurol. Genet.*, **5**, e353.
21. Pratt, B., Fitzgerald, D. and Parker, J. W. (2016) CENTER FOR DRUG EVALUATION AND RISK

ASSESSMENT and RISK MITIGATION REVIEW (S), Niraparib. *CENTER FOR DRUG EVALUATION AND RISK ASSESSMENT and RISK MITIGATION REVIEW (S), Niraparib*; (2016) .

22. Bains, R. K., Sibbons, P. D., Howard, C. V, et al. (1996) Stereological estimation of the absolute number of glomeruli in the kidneys of lambs. **60**, 122–125.
23. Hartman, H. A., Lai, H. L. and Patterson, L. T. (2007) Cessation of renal morphogenesis in mice. *Dev. Biol.*, **310**, 379–387.
24. Neil, E. E. and Bisaccia, E. K. (2019) Nusinersen: A novel antisense oligonucleotide for the treatment of spinal muscular atrophy. *J. Pediatr. Pharmacol. Ther.*, **24**, 194–203.
25. Mendell, J. R., Al-Zaidy, S., Shell, R., et al. (2017) Single-Dose Gene-Replacement Therapy for Spinal Muscular Atrophy. *N. Engl. J. Med.*, **377**, 1713–1722.
26. Seidner, M. (2019) Spinraza® and Zolgensma® for Spinal Muscular Atrophy: Effectiveness and Value Draft Evidence Report. *Spinraza® and Zolgensma® for Spinal Muscular Atrophy: Effectiveness and Value Draft Evidence Report*; (2019) .
27. Luyckx, V., Shukha, K. and Brenner, B. M. (2011) Low Nephron Number and Its Clinical Consequences. *Rambam Maimonides Med. J.*, **2**, e0061.
28. Somers, E., Lees, R. D., Hoban, K., et al. (2016) Vascular Defects and Spinal Cord Hypoxia in Spinal Muscular Atrophy. *Ann. Neurol.*, **79**, 217–230.
29. Somers, E., Stencel, Z., Wishart, T. M., et al. (2012) Density, calibre and ramification of muscle capillaries are altered in a mouse model of severe spinal muscular atrophy. *Neuromuscul. Disord.*, **22**, 435–442.
30. Menendez-Castro, C., Nitz, D., Cordasic, N., et al. (2018) Neonatal nephron loss during active nephrogenesis - Detrimental impact with long-term renal consequences. *Sci. Rep.*, **8**, 4542.
31. Doublier, S., Salvidio, G., Lupia, E., et al. (2003) Nephrin expression is reduced in human diabetic nephropathy: Evidence for a distinct role for glycated albumin and angiotensin II. *Diabetes*, **52**, 1023–1030.
32. Schaefer, L., Ren, S., Schaefer, R. M., et al. (2004) Nephrin expression is increased in anti-Thy1.1-induced glomerulonephritis in rats. *Biochem. Biophys. Res. Commun.*, **324**, 247–254.
33. Wartiovaara, J., Öfverstedt, L. G., Khoshnoodi, J., et al. (2004) Nephrin strands contribute to a porous slit diaphragm scaffold as revealed by electron tomography. *J. Clin. Invest.*, **114**, 1475–1483.
34. Piccinini, E., Kalkkinen, N., Saarma, M., et al. (2013) Glial cell line-derived neurotrophic factor: Characterization of mammalian posttranslational modifications. *Ann. Med.*, **45**, 66–73.
35. Costantini, F. and Shakya, R. (2006) GDNF/Ret signaling and the development of the kidney. *BioEssays*, **28**, 117–127.
36. Rumballe, B. A., Georgas, K. M., Combes, A. N., et al. (2011) Nephron formation adopts a novel spatial topology at cessation of nephrogenesis. *Dev. Biol.*, **360**, 110–122.
37. Hausmanowa-Petrusewicz, I. and Vrbova, G. (2005) Spinal muscular atrophy: a delayed development hypothesis. *Neuroreport*, **16**, 657–661.
38. Hinchliffe, S. A., Lynch, M. R. J., Sargent, P. H., et al. (1992) The effect of intrauterine growth retardation on the development of renal nephrons. *BJOG An Int. J. Obstet. Gynaecol.*, **99**, 296–301.
39. Merlet-Bénichou, C., Gilbert, T., Muffat-Joly, M., et al. (1994) Intrauterine growth retardation leads to a permanent nephron deficit in the rat. *Pediatr. Nephrol.*, **8**, 175–180.
40. Schreuder, M. F. and Nauta, J. (2007) Prenatal programming of nephron number and blood pressure. *Kidney Int.*, **72**, 265–268.
41. McMahon, A. P., Aronow, B. J., Davidson, D. R., et al. (2008) GUDMAP: The genitourinary developmental molecular anatomy project. *J. Am. Soc. Nephrol.*, **19**, 667–671.
42. Pichel, J. G., Shen, L., Sheng, H. Z., et al. (1996) Defects in enteric innervation and kidney development in mice lacking GDNF. *Nature*, **382**, 73–75.
43. Spear, G. S. and Slusser, R. J. (1972) Alport's Syndrome: Emphasizing Electron Microscopic Studies of the Glomerulus. *Am. J. Pathol.*, **69**, 213–224.

44. Cosgrove, D. (2012) Glomerular pathology in Alport syndrome: A molecular perspective. *Pediatr. Nephrol.*, **27**, 885–890.
45. Cosgrove, D. and Liu, S. (2017) Collagen IV diseases: A focus on the glomerular basement membrane in Alport syndrome. *Matrix Biol.*, **57–58**, 45–54.
46. Doné, S. C., Takemoto, M., He, L., et al. (2008) Nephrin is involved in podocyte maturation but not survival during glomerular development. *Kidney Int.*, **73**, 697–704.
47. Li, X., Chuang, P. Y., D'Agati, V. D., et al. (2015) Nephrin preserves podocyte viability and glomerular structure and function in adult kidneys. *J. Am. Soc. Nephrol.*, **26**, 2361–2377.
48. van de Lest, N. A., Zandbergen, M., IJpelaar, D. H. T., et al. (2018) Nephrin Loss Can Be Used to Predict Remission and Long-term Renal Outcome in Patients With Minimal Change Disease. *Kidney Int. reports*, **3**, 168–177.
49. Yuan, H., Takeuchi, E. and Salant, D. J. (2002) Podocyte slit-diaphragm protein nephrin is linked to the actin cytoskeleton. *Am. J. Physiol. - Ren. Physiol.*, **282**, F585–F591.
50. Huwiler, A., Ren, S., Holthöfer, H., et al. (2003) Inflammatory cytokines upregulate nephrin expression in human embryonic kidney epithelial cells and podocytes. *Biochem. Biophys. Res. Commun.*, **305**, 136–142.
51. Wan, B., Feng, P., Guan, Z., et al. (2018) A severe mouse model of spinal muscular atrophy develops early systemic inflammation. *Hum. Mol. Genet.*, **27**, 4061–4076.
52. Wernerson, A., Dunér, F., Pettersson, E., et al. (2003) Altered ultrastructural distribution of nephrin in minimal change nephrotic syndrome. *Nephrol. Dial. Transplant.*, **18**, 70–76.
53. Doublier, S., Ruotsalainen, V., Salvidio, G., et al. (2001) Nephrin redistribution on podocytes is a potential mechanism for proteinuria in patients with primary acquired nephrotic syndrome. *Am. J. Pathol.*, **158**, 1723–1731.
54. Somers, E., Stencel, Z., Wishart, T. M., et al. (2012) Density, calibre and ramification of muscle capillaries are altered in a mouse model of severe spinal muscular atrophy. *Neuromuscul. Disord.*, **22**, 435–442.
55. Araujo, A. prufer de Q. C., Araujo, M. and Swoboda, K. J. (2009) Vascular Perfusion Abnormalities in Infants with Spinal Muscular Atrophy. *J. Pediatr.*, **155**, 292–294.
56. Sariola, H., Saarma, M., Sainio, K., et al. (1991) Dependence of kidney morphogenesis on the expression of nerve growth factor receptor. *Science (80-.).*, **254**, 571–573.
57. Fine, L. G. and Norman, J. T. (2008) Chronic hypoxia as a mechanism of progression of chronic kidney diseases: From hypothesis to novel therapeutics. *Kidney Int.*, **74**, 867–872.
58. Fu, Q., Colgan, S. P. and Shelley, C. S. (2016) Hypoxia: The force that drives chronic Kidney disease. *Clin. Med. Res.*, **14**, 15–39.
59. Puelles, V. G., Hoy, W. E., Hughson, M. D., et al. (2011) Glomerular number and size variability and risk for kidney disease. *Curr. Opin. Nephrol. Hypertens.*, **20**, 7–15.
60. Brenner, B. M., Garcia, D. L. and Anderson, S. (1988) Glomeruli and blood pressure less of one, more the other? *Am. J. Hypertens.*, **1**, 335–347.
61. Brenner, B. M., Lawler, E. V and Mackenzie, H. S. (1996) The hyperfiltration theory: A paradigm shift in nephrology. *Kidney Int.*, **49**, 1774–1777.
62. Gurusinghe, S., Tambay, A. and Sethna, C. B. (2017) Developmental Origins and Nephron Endowment in Hypertension. *Front. Pediatr.*, **5**, 151.
63. Hsieh-Li, H. M., Chang, J.-G., Jong, Y.-J., et al. (2000) A mouse model for spinal muscular atrophy. *Nat. Genet.*, **24**, 66–70.
64. Riessland, M., Ackermann, B., Förster, A. F., et al. (2010) SAHA ameliorates the SMA phenotype in two mouse models for spinal muscular atrophy. *Hum. Mol. Genet.*, **19**, 1492–1506.
65. Nyengaard, J. R. (1999) Stereologic methods and their application in kidney research. *J. Am. Soc. Nephrol.*, **10**, 1100–1123.
66. Rademacher, S., Verheijen, B. M., Hensel, N., et al. (2017) Metalloprotease-mediated cleavage of PlexinD1 and its sequestration to actin rods in the motoneuron disease spinal

muscular atrophy (SMA). *Hum. Mol. Genet.*, **26**, 3946–3959.

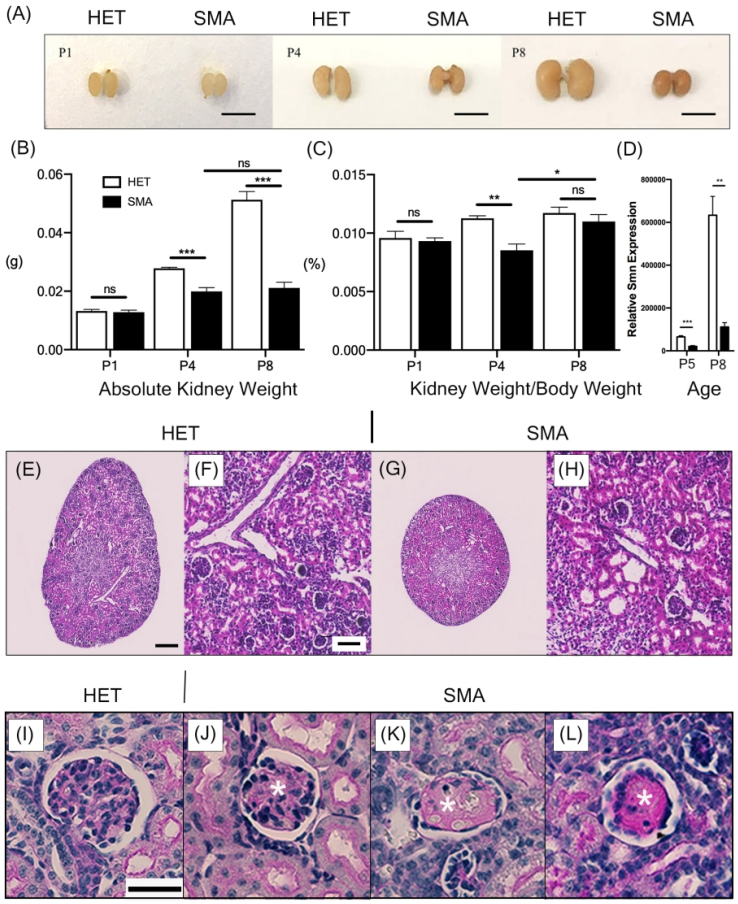

Figure 1: Postnatal kidney development is defective in severe SMA mice.
(A) Gross anatomy of kidneys, harvested from HET (left) and SMA (right) mice at pre-symptomatic (P1), early-symptomatic (P4) and late-symptomatic (P8) stages, respectively. Scale bar, 5mm.
(B) Quantification of kidney weight from P1, P4 and P8 mice. (C) Quantification of kidney weight, relative to body weight from P1, P4 and P8 mice. P values were calculated using a two-tailed Student's t-test. Error bars, mean + S.E.M. (n > 5 mice per group). (D) Relative SMN levels from quantified western blots at P5, ***P, and P8, **P. Error bars, mean + S.E.M. (n > 4 mice per group). (E-H) Representative light microscopy images of entire kidney sections stained with H&E from HET (E) and SMA (G) mice at P8, scale 200μm. Higher magnification images of kidney sections from HET (F) and SMA (H) P8 mice that show no gross morphological abnormalities, scale 100μm. (I-L) Representative photomicrographs of PAS-stained glomeruli from P8 mouse kidneys. (I) Typical healthy glomerulus in P8 HET kidney, (J-L) Glomeruli from kidneys of the SMA mouse model depicting varying degrees of glomerulosclerosis. Increasing accumulation of amorphous, pink, hyaline material shown from minor (J) to major (L), highlighted by asterisk (*). Scale 50μm.

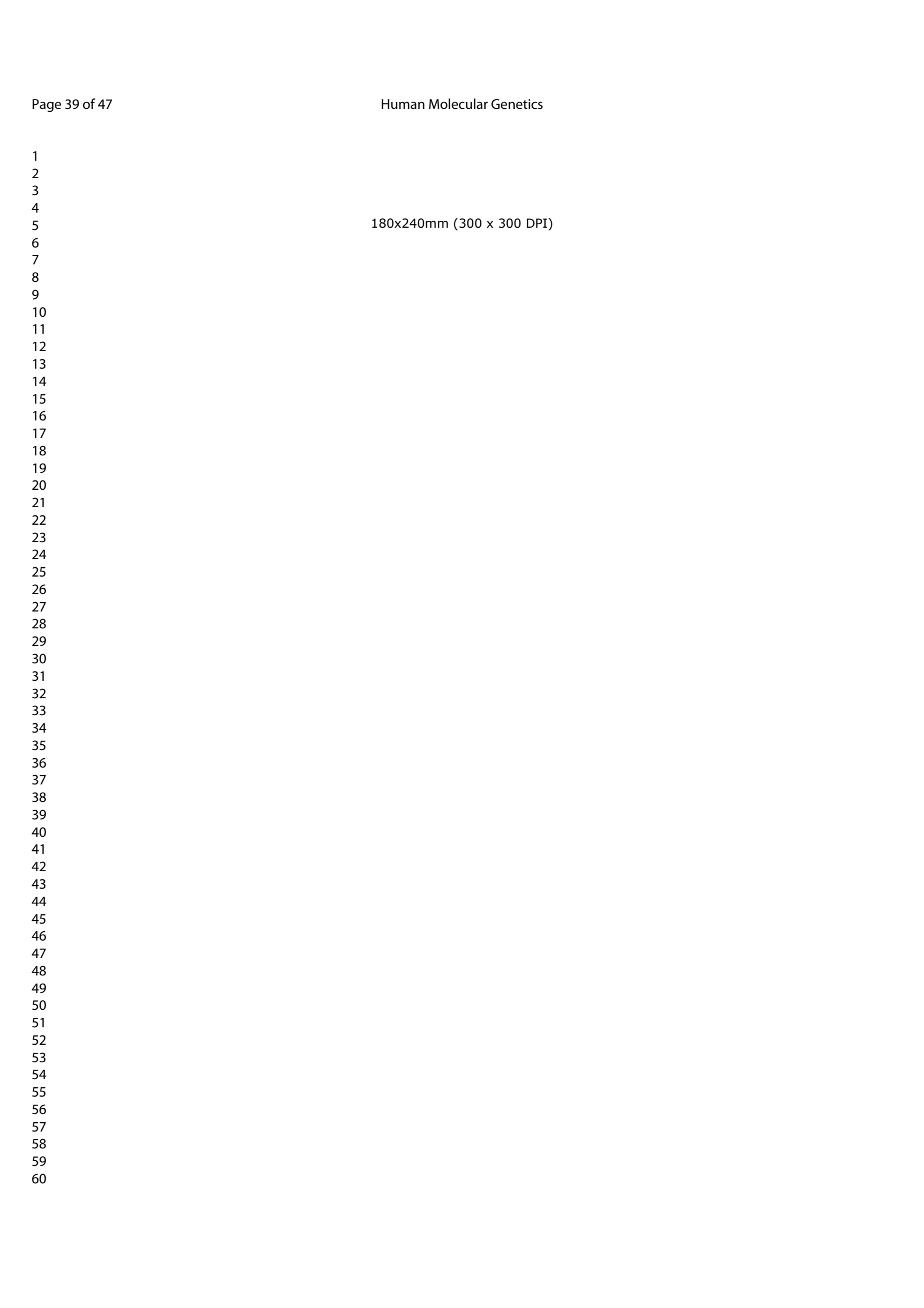
180x240mm (300 x 300 DPI)

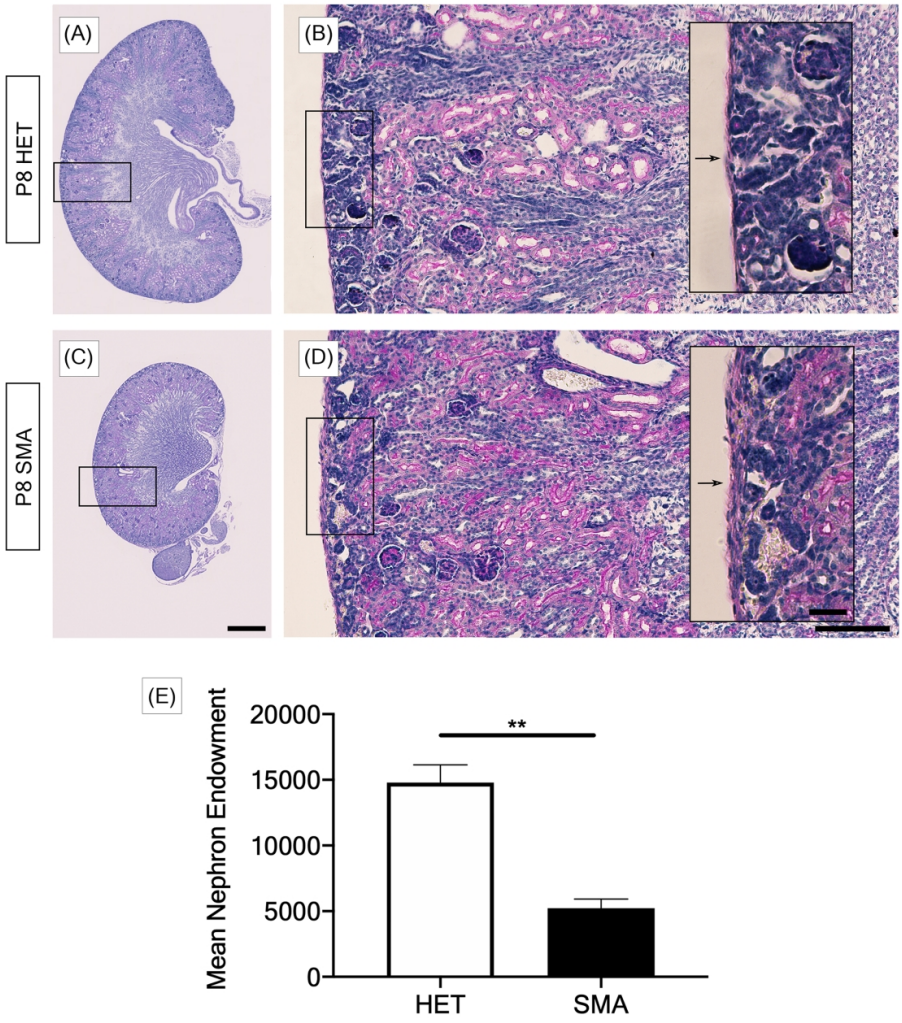

Figure 2: Nephron number is decreased in kidneys from SMA mice

Representative micrographs of PAS stained, coronally sectioned kidneys from HET (A) and SMA (C) P8 mice, scale 0.5mm. Higher magnification images of cortical regions in HET (B) and SMA (D), scale 300μm. Insert depicts lack of nephrons in the peripheral cortex of kidneys from SMA mice and arrow points to thickened renal capsule, scale 150μm. (E) Quantification of nephron number in kidneys of P8 HET and SMA mice, **P. P values were calculated using a two-tailed Student's t-test. Error bars, mean + S.E.M. (n =3 mice per group).

180x207mm (300 x 300 DPI)

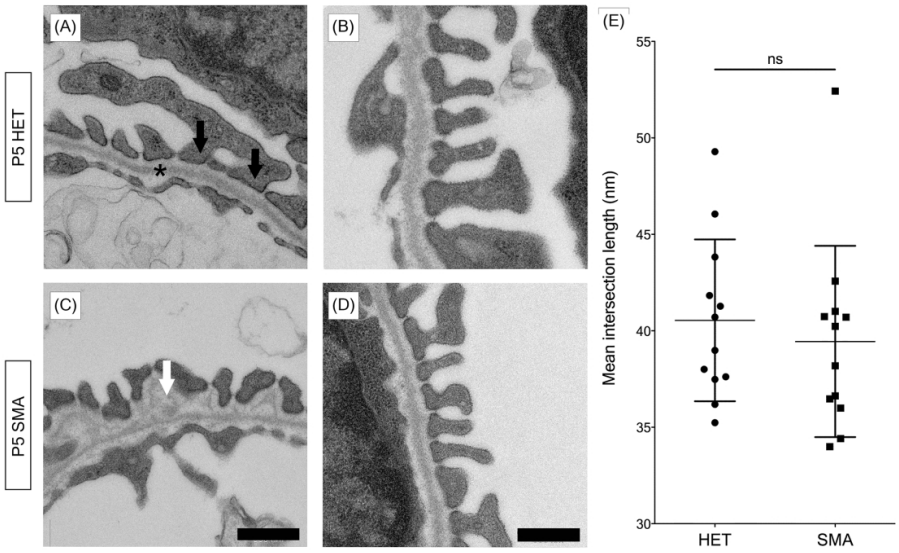

Figure 3: Ultrastructural changes are present in kidneys from SMA mice
Electron micrographs of the basement membrane and podocyte foot processes from P5 kidneys from HET (A) and SMA (C) mice. In (A), black arrows show adjacent foot processes from a single podocyte. The basal lamina is highlighted by an asterisk (*). The white arrow in (C) points to a representative region of glomerular basement lamellation in kidneys from the SMA group. Representative images of P5 kidneys from HET (B) and SMA (D) mice, of podocyte foot processes and underlying basal lamina from which measurements of slit pore length were conducted. Scale 500nm. (E) Quantification of slit membrane length in HET and SMA animals, P=ns. P values were calculated using a two-tailed Student's t-test. Error bars, mean + S.E.M. (n=4 mice per group).

180x117mm (300 x 300 DPI)

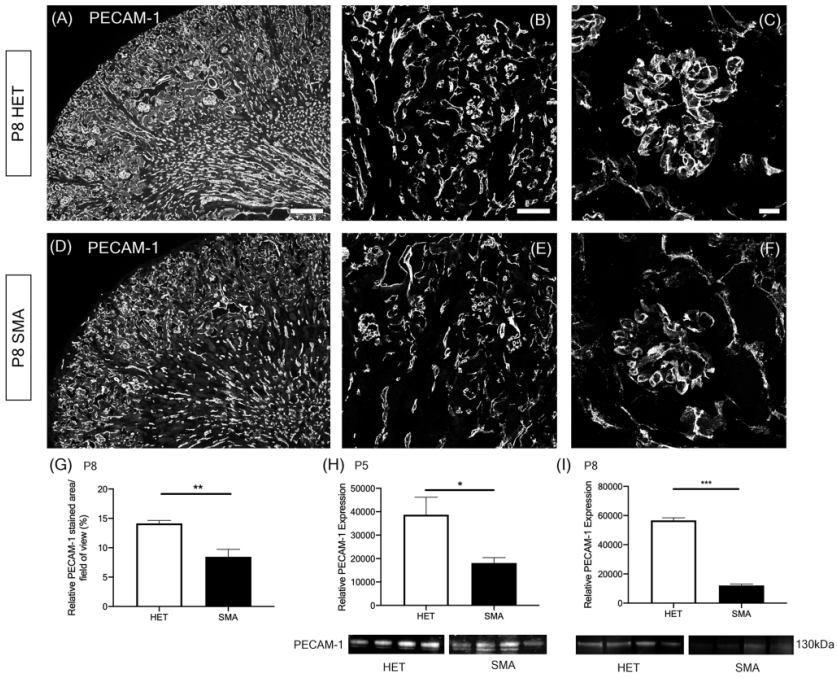

Figure 4: Vascular deficits are evident in kidneys from SMA mice
Representative immunohistochemistry of kidneys from P8 mice, HET (A-C) and SMA (D-F), stained with platelet endothelial cell adhesion marker-1 (PECAM-1). Overview of renal microvasculature in kidneys from HET (A) and SMA (D) P8 mice, highlighting reduction in capillary density and disorganised architecture of vessels, scale 200μm. Higher magnification depicts decreased staining density of renal cortex in SMA (E) compared with HET (B), scale 50μm. Representative z-stack micrographs of glomerular capillary structure in kidneys from HET (C) and SMA (F) animals, depicting less structurally complex capillary loops in SMA mice, scale 10μm. (G) Quantification of staining intensity of PECAM-1. (H-I) Total PECAM-1 protein levels analysed by western blot and normalised to total protein at ages P5 (H), *P, and P8 (I), ***P. P values were calculated using a two-tailed Student's t-test. Error bars, mean + S.E.M. (n >3 mice per group).

180x134mm (300 x 300 DPI)

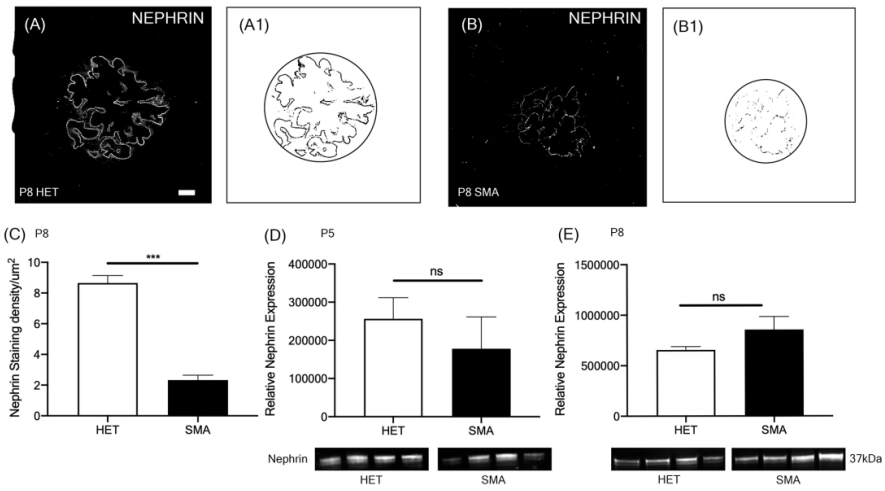

Figure 5: Slit diaphragm protein Nephrin is abnormal in kidneys from SMA mice
Representative immunohistochemistry of kidneys from P8 mice, HET (A) and SMA (B), mature glomeruli are labelled with Nephrin, scale 10μm. (A1-B1) Pixels reversed to show stained (black) area of the glomerulus, encircled to represent glomerular area compared to unstained (white) background from kidneys of P8 HET (A1) and SMA (B1) mice. (C) Quantification of Nephrin stained area. (D-E) Total Nephrin protein levels analysed by western blot and normalised to total protein, at ages P5 (D) and P8 (E), P=ns. P values were calculated using a two-tailed Student's t-test. Error bars, mean + S.E.M. (n >3 mice per group).

180x105mm (300 x 300 DPI)

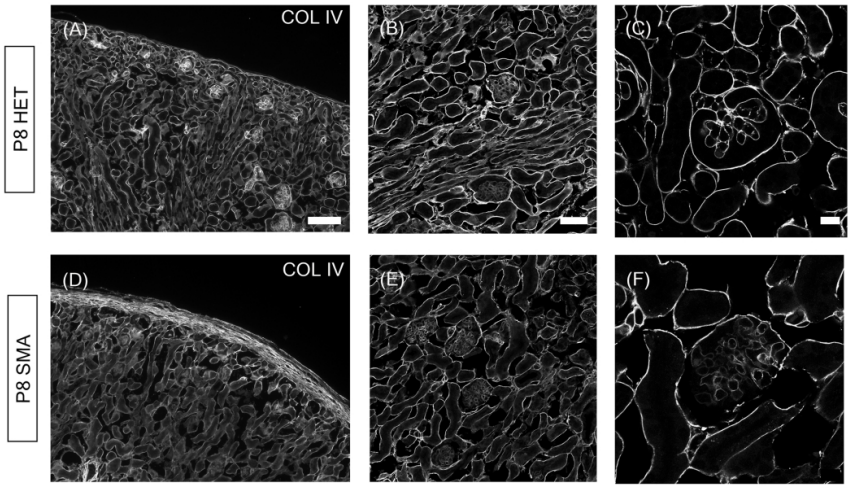

Figure 6: Collagen IV is dysregulated in kidneys from SMA mice
Representative immunohistochemistry of kidneys from P8 mice, HET (A-C) and SMA (D-F), stained with collagen IV. (A and D) Overview of renal cortex and renal capsule. (D) Increased staining density of the renal capsule in kidneys from SMA mice compared to HET (A), scale 100µm. (B and E) Internal glomerular and tubular basement membrane staining density is decreased in kidneys from SMA mice (E), compared to HET (B), scale 50µm. (C and F) Photomicrographs of single glomeruli also further highlight loss of collagen IV expression in glomerular basement membrane in kidneys from SMA mice (F), compared to Het littermates (C), scale 10µm.

180x105mm (300 x 300 DPI)

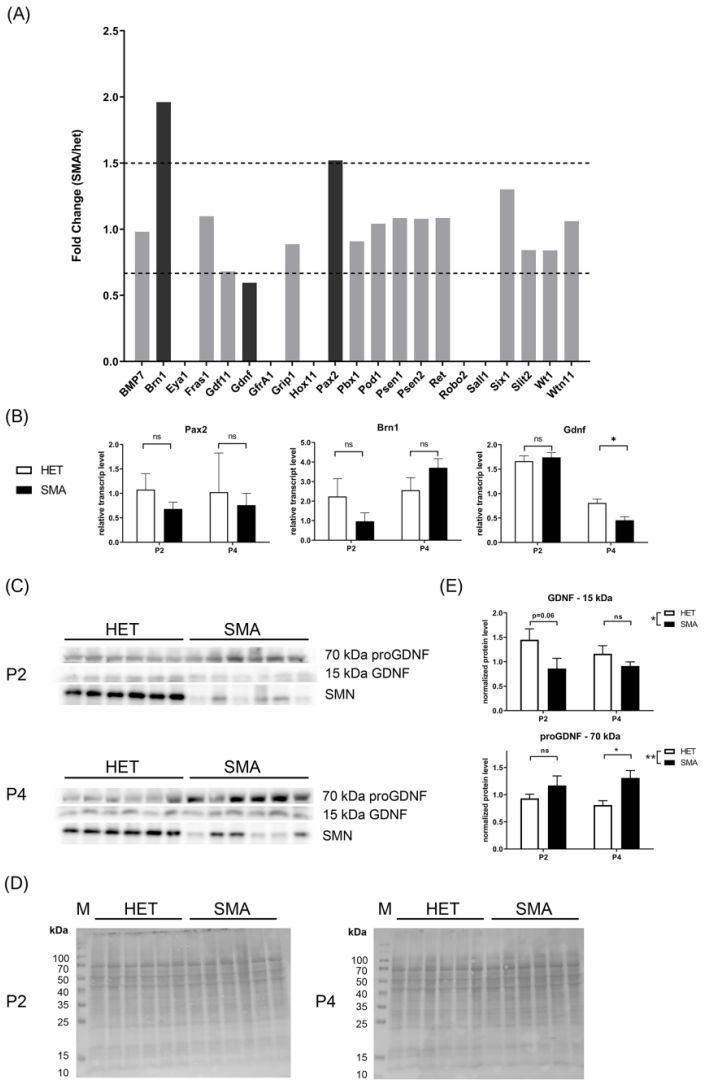

Figure 7: Pre-symptomatic expression of genes and proteins relevant for kidney development
(A) Expression of targets for developmentally-relevant factors were pre-selected by a screening in heterozygous control (HET) and SMA mouse kidneys at P4 by quantitative real time PCR (qRT-PCR). For the screening, pooled samples (for number of samples in the pool, see n-values below) from several mice and litters were used in order to reveal targets with fold changes > 1.5 or < 0.6. Since we applied a screening approach in pooled samples first, no standard deviations were calculated. (B) Three factors found to be regulated in the screening were further analysed by qRT-PCR in individual tissue samples at P2 and P4. Glial cell-line derived growth factor (GDNF) was significantly down-regulated in SMA mice at P4. *P; 2-way ANOVA; Holm-Sidak´s multiple comparisons test; P2 control n=5, P2 SMA n=3, P4 control n=5, P4 SMA n=6. (C) GDNF and SMN protein expression was analysed by Western blotting in HET and SMA kidney samples. Processed GDNF with a relative molecular weight (M) of 15 kDa and an unprocessed pro-form of GDNF (70 kDa) were both detected.
(D) For normalization, membranes were stained with Ponceau S. (D) Densitometic analyses of signals revealed down-regulation of 15 kDa GDNF in SMA samples compared to HER (2way ANOVA with Sidak´s

multiple comparisons; significant for genotype as source of variation, *P, n=6 for each HET and SMA). Moreover, the GDNF pro-form showed an significant upregulation (2way ANOVA with Sidak´s multiple comparisons; significant for genotype as source of variation, **P, n=6 for each HET and SMA; also significant for P4 as time point with *P) indicating an additonal level of regulation by differential proteolytic processing.

180x264mm (300 x 300 DPI)

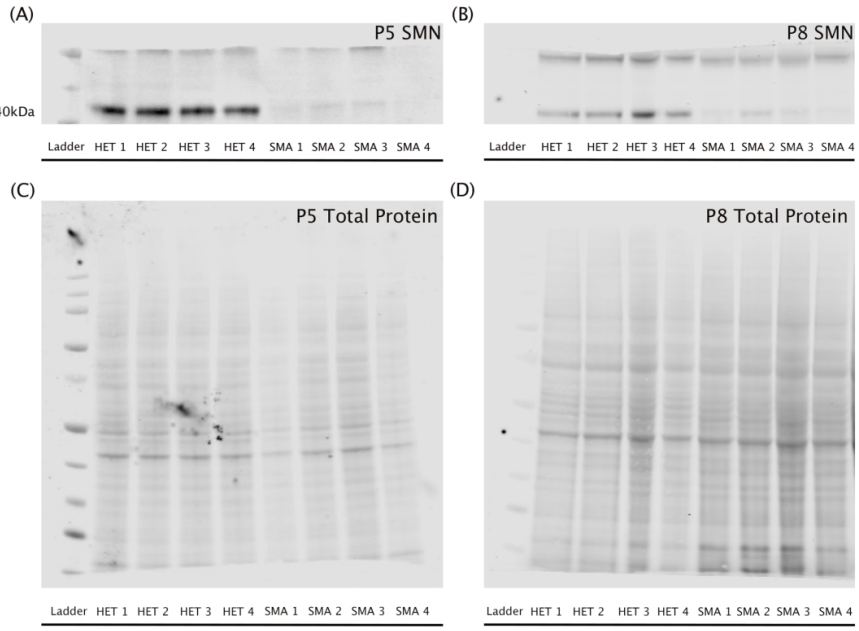

Supplementary Figure 1: SMN Semi-Quantitative Western Blot
Uncropped blots for detection of SMN expression in Het controls and kidneys from SMA mouse model in P5 (A) and P8 (B) animals. Molecular weight of SMN is labelled as 40kDa. Total protein stain was used for normalisation of protein levels and is shown for kidneys from Het controls and SMA mouse model at P5 (C) and P8 (D). n=4 mice per group.

180x132mm (300 x 300 DPI)

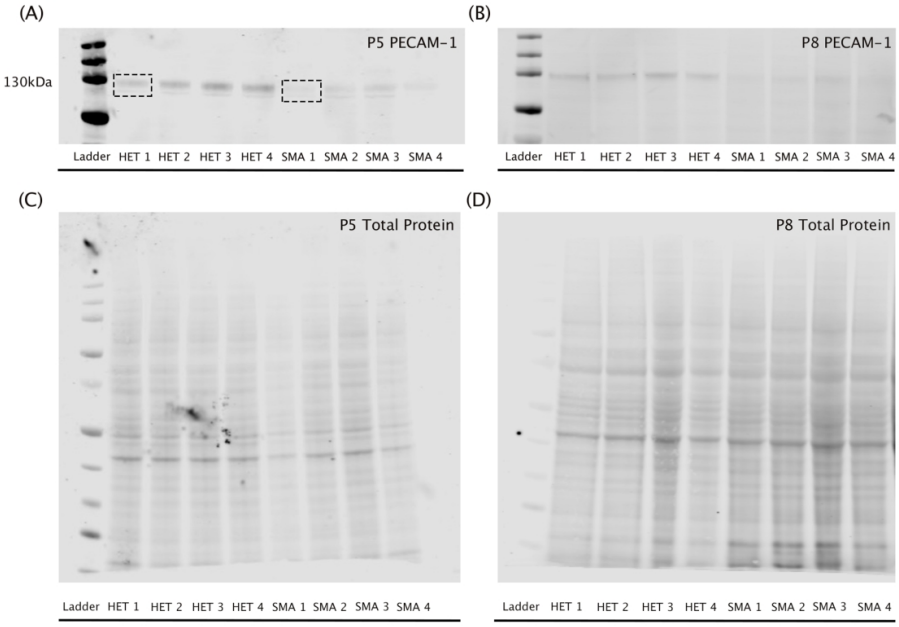

Supplementary Figure 2: PECAM-1 Semi-Quantitative Western Blot
Uncropped blots for detection of PECAM-1 expression in Het controls and kidneys from SMA mouse model in P5 (A) and P8 (B) animals. Molecular weight of SMN is labelled as 130kDa. Boxes highlight area of band quantified in HET 1 and SMA 1 lanes. Both the dominant band and the minor band below was quantified for all lanes. Total protein stain was used for normalisation of protein levels and is shown for kidneys from Het controls and SMA mouse model at P5 (C) and P8 (D). n=4 mice per group.

180x130mm (300 x 300 DPI)

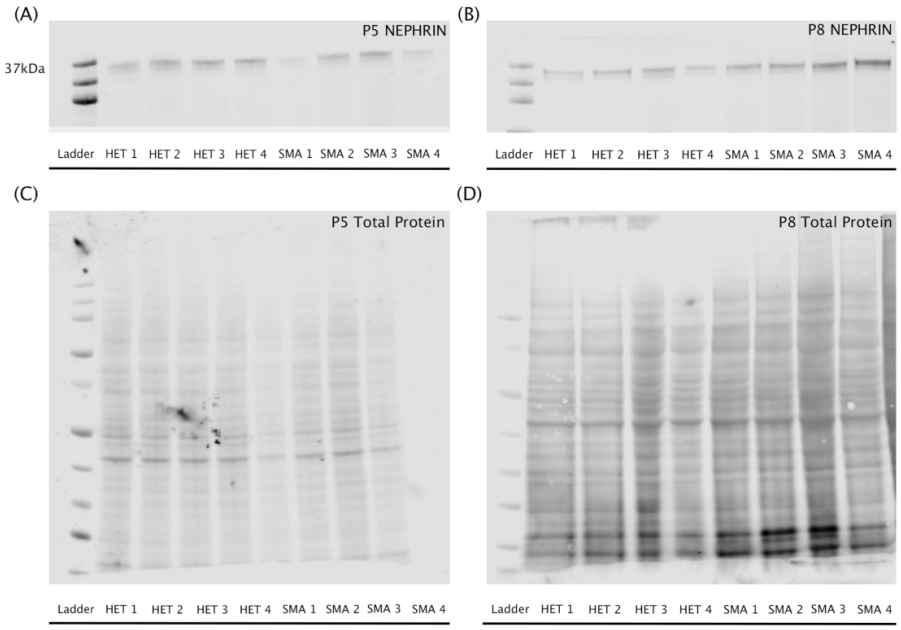

Supplementary Figure 3: Nephrin Semi-Quantitative Western Blot
Uncropped blots for detection of Nephrin expression in Het controls and kidneys from SMA mouse model in P5 (A) and P8 (B) animals. Molecular weight of SMN is labelled as 37kDa. Total protein stain was used for normalisation of protein levels and is shown for kidneys from Het controls and SMA mouse model at P5 (C) and P8 (D). n=4 mice per group.

180x130mm (300 x 300 DPI)